

Determining the planar Nernst effect from magnetic-field-dependent thermopower and resistance in nickel and permalloy thin films

 A. D. Avery,¹ M. R. Pufall,² and B. L. Zink¹
¹*Department of Physics and Astronomy, University of Denver, Denver, Colorado 80208, USA*
²*Electromagnetics Division, National Institute of Standards and Technology, Boulder, Colorado, 80305, USA*

(Received 24 August 2012; published 8 November 2012)

We present magnetic-field-dependent measurements of thermopower, $\alpha(H)$, and resistance, $R(H)$, for Ni₈₀Fe₂₀ and Ni thin films. We conducted these experiments in fields oriented parallel and perpendicular to the applied thermal gradient, $\vec{\nabla}T$, for $\alpha(H)$ and applied current for $R(H)$. We deposited the 20-nm-thick films on 500-nm-thick suspended Si-N thermal isolation platforms that enable in-plane measurements of thermal and electrical properties of thin films. Both $\alpha(H)$ and $R(H)$ in Ni-Fe and Ni films exhibit evidence of spin-dependent scattering through an even field dependence and a linear proportionality between $\alpha(H)$ and $1/R(H)$. Finally, we use $\alpha(H_{\parallel})$ and $\alpha(H_{\perp})$ to determine the planar Nernst coefficient in Ni-Fe and Ni thin films and use this coefficient to predict the size of the planar Nernst effect (PNE) in the micromachined platform. The measured field dependence of the PNE is well matched by the prediction obtained from our $\alpha(H)$ results.

 DOI: [10.1103/PhysRevB.86.184408](https://doi.org/10.1103/PhysRevB.86.184408)

PACS number(s): 72.15.Jf, 72.20.Pa, 72.25.Ba, 73.50.Jt

I. INTRODUCTION

As the size of traditional logic and storage devices continues to be reduced, the effect of heat on micro- and nanoscale samples has become an important research focus for spintronics, spin caloritronics, and thermoelectrics. Careful characterization of thin film properties is necessary for the development of more energy efficient devices and to clarify the underlying physics governing magnetothermoelectric properties of ferromagnetic materials. One such effect is the traditional Seebeck effect, or longitudinal thermopower, where a sample develops a voltage in response to a thermal gradient ($\vec{\nabla}T$) applied across the material.

The longitudinal thermopower of a metal, α , is represented by the Mott equation

$$\alpha(E) = \frac{\pi^2 k_B^2 T}{3e} \left[\frac{1}{\sigma(E)} \frac{\partial \sigma(E)}{\partial E} \right]_{E=E_F}, \quad (1)$$

where σ is the electrical conductivity, E_F is the Fermi energy, and e is the charge of the carrier and is negative for electrons. After simplifying with natural log, separating the bracketed term into two components gives

$$\left[\frac{\partial \ln \sigma(E)}{\partial E} \right]_{E=E_F} = \left[\frac{\partial \ln A}{\partial E} + \frac{\partial \ln \lambda}{\partial E} \right]_{E=E_F}, \quad (2)$$

where A is the area of the Fermi surface and λ is the mean free path of a charge carrier, electron, or hole.¹ The sign and magnitude of α depend on the number of scattered electrons, the type of scattering, and the interaction of the Fermi surface with the Brillouin zone boundary. In fact, the sensitivity of α to charge carrier scattering is apparent in an alternate form of the Mott equation expressed as a function of resistivity ρ :

$$\alpha(E) = -\frac{\pi^2 k_B^2 T}{3e} \frac{1}{\rho(E)} \left[\frac{\partial \rho(E)}{\partial E} \right]_{E=E_F}. \quad (3)$$

The interaction between conduction electrons and sample magnetization adds an additional degree of freedom to the thermoelectric properties of ferromagnetic metals when compared with normal metals. One example of this interac-

tion is the anisotropic magnetoresistance (AMR). In AMR, spin-dependent scattering related to sample magnetization generates a change in $R(H)$. The mean free path of the conduction electrons changes with the orientation of the magnetization relative to the direction of the current flow. This interaction between the conduction electrons and the sample magnetization produces an even field dependence in the sample resistance generated by spin-dependent scattering.² Through $R(H)$, α has an implicit magnetic field dependence along with the energy dependence defined by the Mott equation.

In addition to longitudinal thermopower, ferromagnetic semiconductors and metals exhibit a transverse thermopower also known as the planar Nernst effect (PNE).^{3,4} The PNE is related to the Nernst effect where a magnetic field applied perpendicular to the plane of a sample and a $\vec{\nabla}T$ in the plane of a sample generates an electric field transverse to the applied $\vec{\nabla}T$. In contrast to the Nernst effect, the planar Nernst effect depends on the angle between the in-plane sample magnetization and the $\vec{\nabla}T$. In the PNE, the resulting electric field is transverse to the direction of the applied $\vec{\nabla}T$. The PNE coefficient is defined by³

$$\alpha_{\text{PNE}}(H) = \frac{1}{2} [\alpha(H_{\parallel}) - \alpha(H_{\perp})] \sin 2\theta. \quad (4)$$

In this equation, $\alpha(H_{\parallel})$ and $\alpha(H_{\perp})$ are longitudinal thermopower coefficients measured in external fields oriented parallel and perpendicular to the applied $\vec{\nabla}T$. θ is the angle between the film magnetization, \vec{M} , and $\vec{\nabla}T$. The resulting angular dependence of the PNE is proportional to $\sin 2\theta$.

The spin Seebeck effect is another effect thought to be generated by a $\vec{\nabla}T$ and detected by measuring a transverse voltage, V_T .⁵⁻⁷ In the SSE, a $\vec{\nabla}T$ applied across a sample is said to produce a pure spin current that is detected by measuring the V_T generated through the inverse spin Hall effect. In contrast to the PNE, the SSE is predicted to have a cosine dependence on the angle between \vec{M} and $\vec{\nabla}T$, making it possible to distinguish between these effects using their angular dependence. We recently conducted an experiment designed to measure the SSE in a geometry that limited the $\vec{\nabla}T$ to the plane of the sample film. However, rather than

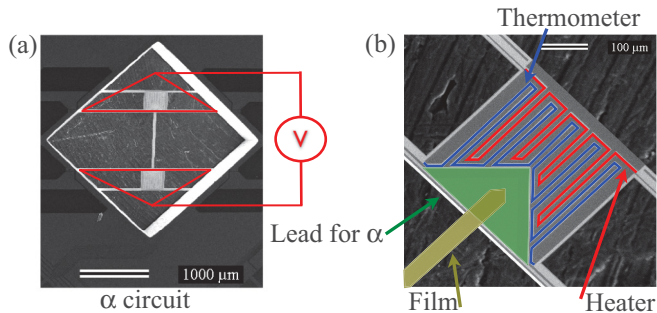


FIG. 1. (Color online) (a) Scanning electron micrograph of a thermal isolation platform with the α circuit shown schematically. (b) SEM micrograph zoom of one island with leads and film highlighted in false color.

the SSE, we observed the $\sin 2\theta$ dependence generated by the PNE.⁸

Previous studies have explored $\alpha(H)$ in magnetic tunnel junctions,⁹ multilayered thin films,^{10–13} and multilayered nanowires.^{14,15} However, few studies have probed single-layer thin films. In this paper, we present $R(H)$, $\alpha(T)$, and $\alpha(H)$ measurements made on single-layer 20-nm-thick Ni and Ni-Fe films that are supported by suspended Si-N thermal isolation platforms. We show that the magnetic field dependence for both R and α originates from spin-dependent scattering. Finally, we compare our previous PNE results to the PNE coefficient calculated from the $\alpha(H)$ results, confirming that the origin of the PNE is also spin-dependent scattering.

II. EXPERIMENTAL DETAILS

We previously measured $\alpha(T)$, resistivity, and in-plane thermal conductivity of thin films using earlier versions of our thermal isolation platforms.^{16,19} However, we conducted our current experiments using an updated platform design that includes a platinum lead at each end of the film. As well as longitudinal thermopower, we can now measure transverse thermopower using these additional leads. We fabricated the platforms and films for this experiment and our PNE experiments⁸ at the same time on a single Si-N coated silicon wafer. The thermal platforms used for the current data have the exact same design and geometry as those used for the PNE experiment.²⁰

We fabricate suspended thermal isolation platforms using 500-nm-thick low-stress Si-N. An SEM micrograph of an example platform and a schematic of our α measurement circuit are shown in Fig. 1. Each platform has two islands with integrated heaters and thermometers for applying, maintaining, and measuring temperature gradients. An $800 \times 35\text{-}\mu\text{m}$ bridge connects the islands and serves both as support for a deposited film and as the only thermal link between the two islands. The platform is suspended and connected to a Si frame by eight Si-N legs. Fabrication and deposition details are published elsewhere.⁸ To prevent convective heating, we make all measurements in a sample-in-vacuum cryostat at pressures of 10^{-5} to 10^{-6} torr. We mount the thermal isolation platforms to a gold-plated copper block and wire bond to make connections to room-temperature electronics. A radiation shield encloses the platform before it is inserted into the cryostat to prevent radiative heating.

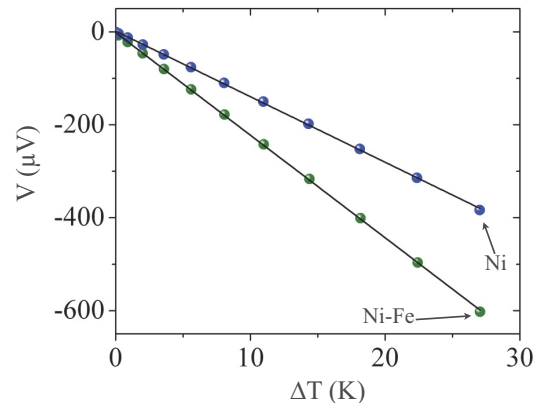


FIG. 2. (Color online) ΔT dependence of the voltage generated in response to an applied thermal gradient for Ni-Fe and Ni films with linear fits displayed as solid lines. The slope from the linear fit to the data gives α .

Figure 2 shows an example data point for 20-nm-thick Ni-Fe and Ni films at 276 K. To determine α , we measure the thermovoltages generated in response to a series of applied powers and plot V versus ΔT . α is the slope of the linear fit to the V versus ΔT plot at each reference temperature. We measured $\alpha(T)$ from 77 to 325 K. All $\alpha(H)$ and $R(H)$ measurements were conducted at a base temperature of 276 K. For $\alpha(H)$ and $R(H)$, we swept an external magnetic field (H) between ± 200 Oe. We applied the external field parallel or perpendicular to the applied I or $\vec{\nabla}T$. We converted measured R into resistivity, ρ , using the known geometry of the films ($\rho = RA/L$).

III. RESULTS AND DISCUSSION

Figure 3 shows α versus temperature at $H = 0$ for a Ni film and a Ni-Fe film compared to previous measurements of similar thin films and to bulk samples.^{17,18} The room

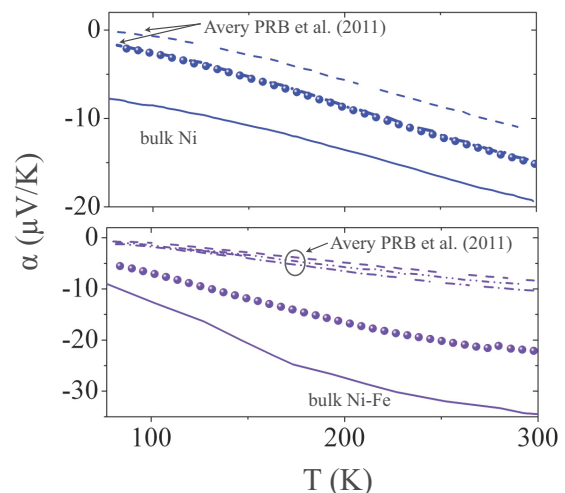


FIG. 3. (Color online) Temperature dependence of α for a 20-nm-thick Ni (top panel) and a Ni-Fe (bottom panel) film (circles) compared to previously measured films¹⁶ (dotted lines) and bulk literature values (solid lines) for Ni¹⁷ and Ni-Fe.¹⁸

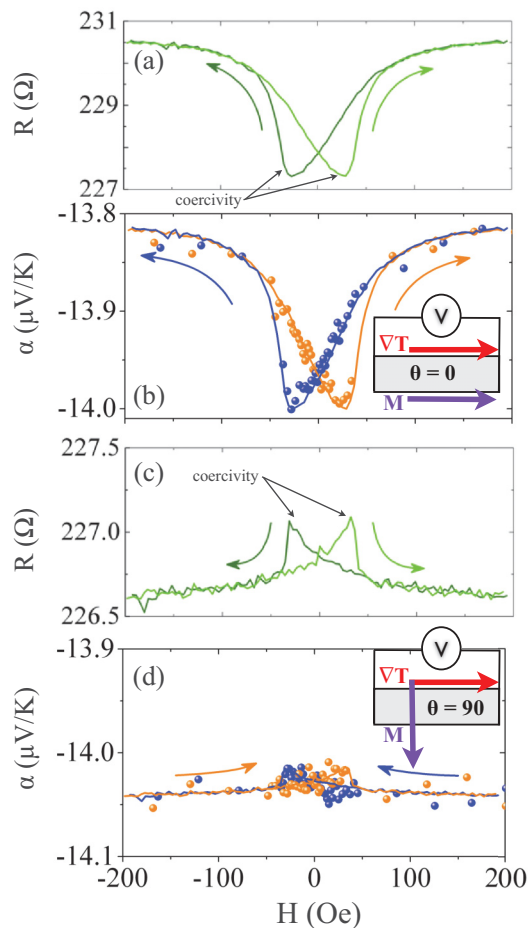


FIG. 4. (Color online) Magnetic field dependence of R and α for a 20 nm thick Ni film. (a) $R(H_{\parallel})$, (b) $\alpha(H_{\parallel})$, (c) $R(H_{\perp})$, and (d) $\alpha(H_{\perp})$. Solid lines in (b) and (d) represent $\alpha(H)$ values predicted using linear fits to the α vs $1/R$ plot for Ni. All measurements are made at a base temperature of 276 K.

temperature α value for our Ni-Fe matches the α value for $\text{Ni}_{81}\text{Fe}_{19}$ from an earlier experiment reporting the SSE in ferromagnetic metals by Uchida *et al.*⁵ The temperature dependence of α for both films is similar to 60- to 167-nm-thick films measured on an earlier version of our thermal isolation platform using the same technique.¹⁶ With one exception, the α and ρ values for the current 20-nm-thick films are closer to bulk values than previous films. The 20-nm Ni film has the same $\alpha(T)$ as a 50-nm-thick Ni film previously grown in the same chamber. This confirms that any increase in $\alpha(T)$ magnitude toward bulk values stems from fewer defects and impurities in our current films rather than a thickness dependence, as expected. Electrons dominate conduction in Ni and Ni-Fe alloys,²¹ resulting in the observed negative α for both Ni and Ni-Fe.

Figure 4 shows $R(H)$ and $\alpha(H)$ of a Ni film for external magnetic fields applied parallel (H_{\parallel}) and perpendicular (H_{\perp}) to I or ∇T . To differentiate, we denote $R(H_{\parallel})$, $\alpha(H_{\parallel})$, $R(H_{\perp})$, and $\alpha(H_{\perp})$. From $R(H)$ measurements, we determine the Ni film coercivity is ≈ 30 Oe. The $R(H_{\parallel})$ and $R(H_{\perp})$ data confirm that the film magnetization switches as the field is swept. As the film \vec{M} sweeps from fully saturated

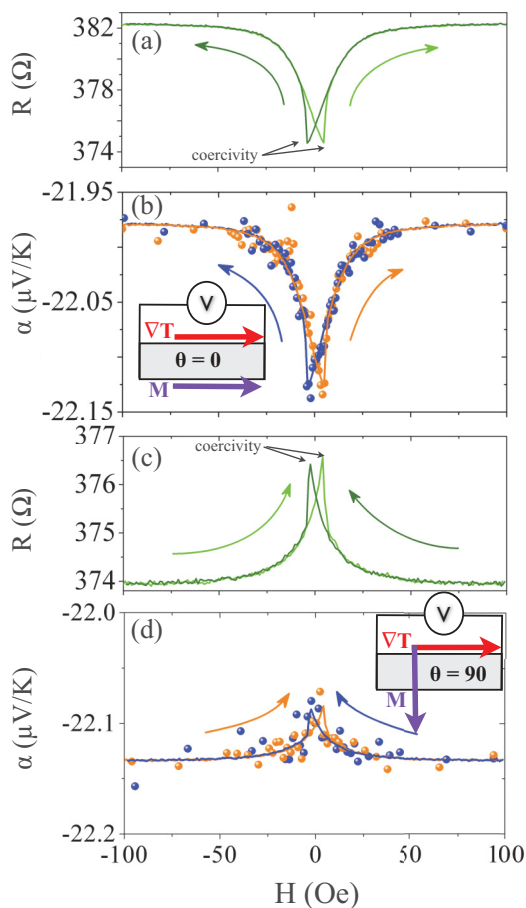


FIG. 5. (Color online) Magnetic field dependence of R and α for a 20 nm thick Ni-Fe film. (a) $R(H_{\parallel})$, (b) $\alpha(H_{\parallel})$, (c) $R(H_{\perp})$, and (d) $\alpha(H_{\perp})$. Solid lines in (b) and (d) represent $\alpha(H)$ values predicted using linear fits to the α vs $1/R$ plot for Ni-Fe. All measurements are made at a base temperature of 276 K.

to $\vec{M} \approx 0$, $R(H_{\parallel})$ decreases and $R(H_{\perp})$ increases, shown in Figs. 4(a) and 4(c). Both $R(H_{\parallel})$ and $R(H_{\perp})$ exhibit an even field dependence, indicating spin-dependent scattering in the presence of magnetic domains oriented both parallel and perpendicular to the applied current when \vec{M} is zero.

Figures 4(b) and 4(d) show $\alpha(H_{\parallel})$ and $\alpha(H_{\perp})$ for the Ni film. The coercivity for both $\alpha(H_{\parallel})$ and $\alpha(H_{\perp})$ is ≈ 30 Oe as expected from the $R(H)$ data. The $\alpha(H_{\parallel})$ magnitude increases as H_{\parallel} is reduced from saturation to coercivity, correlating with the decrease seen in $R(H_{\parallel})$. Likewise, the magnitude of $\alpha(H_{\perp})$ decreases as $R(H_{\perp})$ increases. $\alpha(H)$ and $R(H)$ display an inverse proportionality predicted by Eq. (3) only if the remaining terms on the right-hand side are constant. The $\alpha(H)$ data trace the $R(H)$ data in both orientations, suggesting that spin-dependent scattering is the common physical origin.

$R(H)$ and $\alpha(H)$ for a 20-nm-thick Ni-Fe film are displayed in Fig. 5. For Ni-Fe, both the $R(H)$ and $\alpha(H)$ for parallel and perpendicular external fields exhibit a coercivity ≈ 5 Oe. Like Ni, Ni-Fe \vec{M} switches with field and both parallel and perpendicular domains are present at $|\vec{M}| = 0$. However, Ni-Fe has a smaller coercivity than Ni, as expected. As with Ni, Ni-Fe $\alpha(H)$ also increases(decreases) as $R(H)$ decreases(increases),

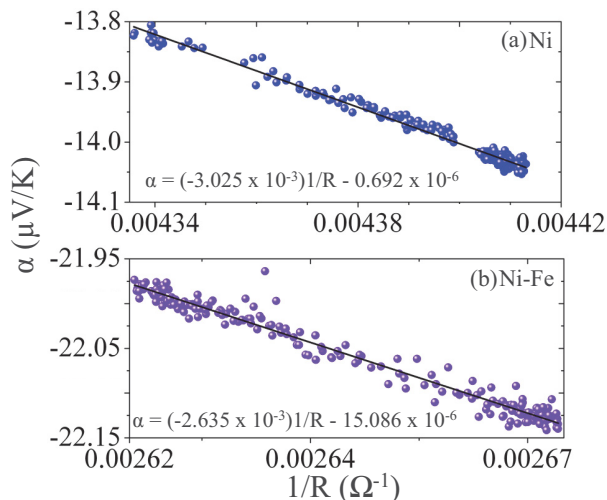


FIG. 6. (Color online) Inverse R dependence of α for (a) Ni and (b) Ni-Fe films measured in H_{\parallel} and H_{\perp} . Solid lines represent linear fits to the data.

suggesting that $\alpha(H)$ and $R(H)$ for Ni-Fe are related through spin-dependent scattering.

For quantitative evidence of spin-dependent scattering in α , we convert ρ in Eq. (3) to R and examine $\alpha(1/R)$. Figure 6 shows α versus $1/R$ plots for Ni and Ni-Fe and a linear fit for each. Once the proportionality between α and $1/R$ is determined, we generate the expected $\alpha(H)$ values and plot them as solid lines in Figs. 4(b) and 4(d) for Ni and Figs. 5(b) and 5(d) for Ni-Fe. The predicted $\alpha(H)$ lines for Ni and Ni-Fe follow the observed shape of the actual data. This illustrates the direct proportionality between $\alpha(H)$ and $1/R(H)$. The remaining terms in Eq. (3) ($\pi^2 k_B^2 T / 3e [\partial \rho(E) / \partial E]_{E=E_F}$) are independent of H at a given temperature. Therefore, like $R(H)$, the magnetic field dependence of α for a given temperature is due to spin-dependent scattering.

Finally, we compare our results for α and Eq. (4) to the PNE measurement from our previous experiments.⁸ In these experiments, we applied a magnetic field at an angle to $\vec{\nabla}T$, for example 45° . Next, we swept the field from positive 200 Oe to negative 200 Oe and measured the resulting V_T . This reversed the direction of the field vector resulting in a 225° angle with the $\vec{\nabla}T$. We switched between 135° and 315° using the same method. To calculate V_T , first we determine the transverse thermopower coefficient (α_{PNE}) using Eq. (4). Since θ is only well-defined at saturation, we use the saturated values $\alpha(H_{\parallel} = 200 \text{ Oe}) = -13.83 \mu\text{V/K}$ and $\alpha(H_{\perp} = 200 \text{ Oe}) = -14.03 \mu\text{V/K}$ for Ni to determine α_{PNE} for all θ . We repeat the process to determine α_{PNE} for Ni-Fe as well. Figure 7(a) shows the angular dependence of α_{PNE} for Ni and Ni-Fe for comparison. Although Ni α is smaller than Ni-Fe α at 276 K, we calculate a larger α_{PNE} for Ni than Ni-Fe at 276 K.

Next, we use α_{PNE} to determine V_T . Like the longitudinal thermopower, the transverse thermopower generates an electric field from an applied $\vec{\nabla}T$. In the longitudinal thermopower, the electric field (\vec{E}) is generated over the same geometry as the $\vec{\nabla}T$. These dimensions cancel, leaving a voltage and a ΔT . In the transverse thermopower, $\vec{\nabla}T$ is applied perpendicular

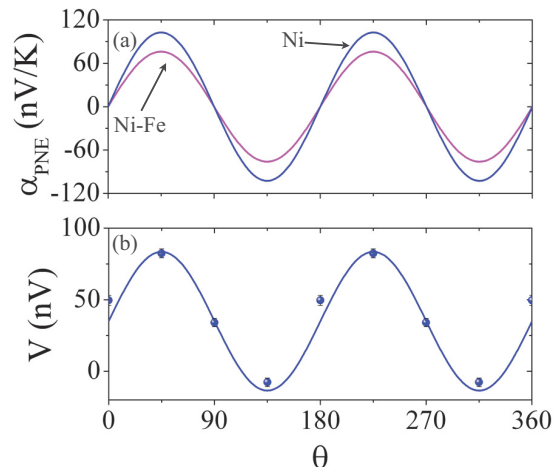


FIG. 7. (Color online) (a) Angular dependence of the calculated PNE coefficients (α_{PNE}) for Ni-Fe and Ni generated using Eq. (4). (b) Angular dependence of the expected voltage from Ni (solid line) compared with the voltage generated by the PNE from Avery *et al.*⁸ for a 20-nm Ni film deposited at the same time as the Ni sample from this experiment.

to the resulting \vec{E} field,

$$E_y = \frac{V_T}{w} = \alpha_{\text{PNE}} \frac{\Delta T}{L}. \quad (5)$$

In this equation, w is the width of the film, L is the length, and ΔT the temperature difference along the length of the film. This results in an equation that can be solved for the expected transverse voltage (V_T) generated by the PNE. In our experiment, the Pt lead and other metal features partially shorted the ferromagnetic film. This short reduces the expected V_T by a factor we introduce as a free parameter. This parameter depends on the resistivity and geometry of the Pt, Mo, and ferromagnetic layers as well as the quality of their interface. In order to match the data, the value of the free parameter in our experiment is 0.4. Finally, in the original PNE experiments we measured a V_T offset at both $\theta = 0^\circ$ and $\theta = 90^\circ$, where PNE is predicted to be zero. PNE data at all other θ appeared to be shifted by this offset as well. To account for the offset, we added the 35 nV offset measured at $\theta = 90^\circ$ in the original PNE experiments. Figure 7(b) shows the calculated PNE V_T for $\theta = 0^\circ$ to 360° plotted as a solid line and compared to data from a 20-nm Ni film grown at the same time as our current samples.

Figure 8 shows the magnetic field dependence of previously measured V_T and predicted $V_T(H)$. To predict $V_T(H)$ we determined α_{PNE} for all applied H between ± 200 Oe and $\theta = 45^\circ, 135^\circ, 225^\circ$, and 315° . We determined V_T from the known geometry, ΔT and α_{PNE} , multiplied by 0.4, and added the 35-nV offset. As mentioned earlier, the PNE equation is well-defined only when the film is fully saturated. Between $\pm H_{\text{sat}}$, \vec{M} is undefined (indicated by dotted lines in Fig. 8). However, the Eq. (4) prediction reproduces the shape and magnitude of the previously measured PNE along the entire range of applied external field. This close prediction in the intermediate regime, where \vec{M} is undefined, suggests there is a roughly equal volume of parallel and perpendicular domains over the entire film at field values less than saturation, even

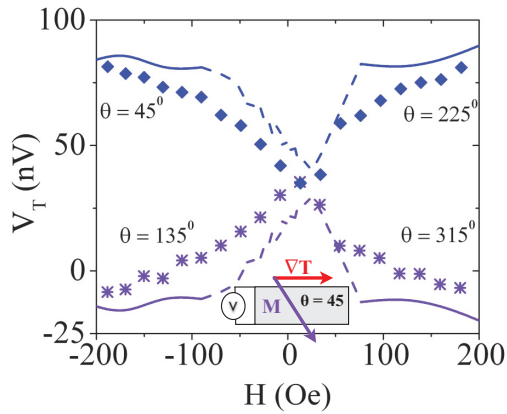


FIG. 8. (Color online) Magnetic field dependence of the V_T generated by the transverse thermopower (or planar Nernst effect) for a 20-nm-thick Ni film¹⁶ at $\theta = 45^\circ, 135^\circ, 225^\circ, 315^\circ$. The solid lines represent the voltage predicted using $\alpha(H_{\parallel})$ and $\alpha(H_{\perp})$, where the film is saturated. Dotted lines represent the prediction where \vec{M} is not well-defined.

though individual domain orientation will differ from one field sweep to the next. The predicted PNE V_T has both an angular dependence and a magnetic field dependence that agrees very well with the experimental data. From this agreement, we conclude that the transverse thermopower originates from spin-dependent scattering as well.

Since the origin of the planar Nernst effect is the same spin-dependent scattering responsible for not only longitudinal thermopower but AMR as well, a PNE component should be found in any experiment measuring transverse voltages on ferromagnets that display AMR. For example, using α_{PNE} shown in Fig. 7(a), a Ni-Fe sample with the same AMR and

α , with sample width of 4 mm and length of 6 mm with an applied longitudinal temperature difference of 20 K should display a transverse voltage with $\sin 2\theta$ angular dependence and maximum value of $0.9 \mu\text{V}$.

IV. CONCLUSION

We have presented measurements of $\alpha(T)$, $\alpha(H)$, and $R(H)$ of 20-nm-thick Ni and Ni-Fe films. The temperature dependence of α for both materials was similar to previously published results for thin films measured using the same technique on an earlier version of the supporting platform. However, the 20-nm films displayed a lower resistance than previous films, resulting in $\alpha(T)$ values closer to bulk values. Ni and Ni-Fe films exhibited even magnetic field dependence for $\alpha(H)$ and $R(H)$. We observed a coercivity of ≈ 30 Oe for Ni and ≈ 5 Oe for Ni-Fe. Both Ni-Fe and Ni exhibit a linear proportionality between α and $1/R$ predicted by the Mott equation. Thus, for a given temperature, α is a function of ρ and the $(\partial\rho/\partial E)_{E=E_F}$ term is constant. Finally, we used $\alpha(H_{\parallel})$ and $\alpha(H_{\perp})$ to predict previous PNE results of films grown during the same deposition. From the even-field dependence of both $\alpha(H)$ and $R(H)$, the linear relationship between α and $1/R$, and the prediction of PNE results using $\alpha(H_{\parallel})$ and $\alpha(H_{\perp})$, we conclude all three share a common physical origin of spin-dependent scattering.

ACKNOWLEDGMENTS

We gratefully acknowledge support from the NSF CAREER Grant (No. DMR-0847796). We also thank J. Beall, G. Hilton, D. Schmidt, and A. Fox for fabrication advice and assistance, and S. Mason, D. Bassett, and G. Cotteril for assistance in the lab.

- ¹J. M. Ziman, *Electrons and Phonons* (Oxford University, London, 1960).
- ²R. C. O'Handley, *Modern Magnetic Materials: Principles and Applications* (John Wiley & Sons, New York, 2000).
- ³Y. Pu, E. Johnston-Halperin, D. D. Awschalom, and J. Shi, *Phys. Rev. Lett.* **97**, 036601 (2006).
- ⁴V. Ky, *Phys. Status Solidi B* **22**, 729 (1967).
- ⁵K. Uchida, S. Takahashi, K. Harii, J. Ieda, W. Koshibae, K. Ando, S. Maekawa, and E. Saitoh, *Nature (London)* **455**, 778 (2008).
- ⁶J. Sinova, *Nat. Mater.* **9**, 880 (2010).
- ⁷C. M. Jaworski, J. Yang, S. Mack, D. D. Awschalom, J. P. Heremans, and R. C. Myers, *Nat. Mater.* **9**, 898 (2010).
- ⁸A. D. Avery, M. R. Pufall, and B. L. Zink, *Phys. Rev. Lett.* (to be published).
- ⁹N. Liebing, S. Serrano-Guisan, K. Rott, G. Reiss, J. Langer, B. Ocker, and H. W. Schumacher, *Phys. Rev. Lett.* **107**, 177201 (2011).
- ¹⁰M. Conover, M. Brodsky, J. Mattson, C. Sowers, and S. Bader, *J. Magn. Magn. Mater.* **102**, L5 (1991).
- ¹¹L. Piraux, A. Fert, P. A. Schroeder, R. Loloee, and P. Etienne, *J. Magn. Magn. Mater.* **110**, L247 (1992).
- ¹²J. Shi, S. S. P. Parkin, L. Xing, and M. B. Salamon, *J. Magn. Magn. Mater.* **125**, L251 (1993).
- ¹³J. Shi, K. Pettit, E. Kita, S. S. P. Parkin, R. Nakatani, and M. B. Salamon, *Phys. Rev. B* **54**, 15273 (1996).
- ¹⁴L. Gravier, A. Fábíán, A. Rudolf, A. Cachin, J.-E. Wegrowe, and J.-P. Ansermet, *J. Magn. Magn. Mater.* **271**, 153 (2004).
- ¹⁵S. Serrano-Guisan, L. Gravier, M. Abid, and J.-P. Ansermet, *J. Appl. Phys.* **99**, 08T108 (2006).
- ¹⁶A. D. Avery, R. Sultan, D. Bassett, D. Wei, and B. L. Zink, *Phys. Rev. B* **83**, 100401 (2011).
- ¹⁷F. J. Blatt, D. J. Flood, V. Rowe, P. A. Schroeder, and J. E. Cox, *Phys. Rev. Lett.* **18**, 395 (1967).
- ¹⁸C. Y. Ho, T. C. Chi, R. H. Bogaard, T. N. Havill, and H. M. James, in *Thermal Conductivity 17*, Vol. 17, edited by J. G. Hust (Plenum Press, New York, 1983), pp. 195–205.
- ¹⁹R. Sultan, A. D. Avery, G. Stiehl, and B. L. Zink, *J. Appl. Phys.* **105**, 043501 (2009).
- ²⁰Note that the Pt strip on the top of the sample film is not required for a transverse thermopower measurement. All platforms used in our experiments so far do have this strip, which was designed to test for thermally generated spin currents via the inverse spin Hall effect.
- ²¹S. Soffer, J. A. Dressen, and E. M. Pugh, *Phys. Rev.* **140**, A668 (1965).